International Journal of Mass Spectrometry 306 (2011) 196–203

Contents lists available at ScienceDirect

International Journal of Mass Spectrometry

journal homepage: www.elsevier.com/locate/ijms

# Two-dimensional FT-ICR/MS with IRMPD as fragmentation mode

Maria A. van Agthoven[a], Marc-André Delsuc[b], Christian Rolando[a,*]

[a] USR CNRS 3290 Miniaturisation de Systèmes d'Analyse et de Protéomique and FR CNRS 2638 Institut Michel-Eugène Chevreul, Université de Lille 1, Sciences et Technologie, Villeneuve d'Ascq, France
[b] Institut de Génomique et de Biologie Moléculaire et Cellulaire, Illkirch-Graffenstaden, France

ARTICLE INFO

*Article history:*
Received 27 August 2010
Received in revised form 22 October 2010
Accepted 27 October 2010
Available online 12 November 2010

*Keywords:*
FT-ICR
2-Dimensional
IRMPD
FTMS
Pulse sequence
Double-frequency

ABSTRACT

In 1988, Gäumann et al. introduced a pulse sequence for two-dimensional FT-ICR/MS correlating parent ions and fragment ions without the need for ion isolation. The improvement in computer technology makes this pulse sequence analytically useful in order to obtain structural information on complex samples. The pulse sequence can be applied to all cyclotron radius-dependent fragmentation modes, including gas-free fragmentation modes like IRMPD, which do not affect sensitivity and resolving power like the pulsing of a gas into the ICR cell does. This study shows the feasibility of 2D FT-ICR/MS and lays the groundwork to turn this method into a viable analytical tool.



## 1. Introduction

Two-dimensional FT-ICR/MS [1] was first introduced by Gäumann et al. in 1987 in order to study ion-molecule reactions and fragmentations in an ICR cell [2–5]. It was based on an experiment by Marshall et al. in 1984 [6] proving that it is possible to de-excite ion packets in the ICR cell. The 2D FT-ICR/MS experiment was modeled after NOESY spectroscopy in 2D-NMR [7].

By comparing the relative ICR magnitude after an increasingly long excitation pulse and a pulse with a phase inversion after 1 ms, Marshall's experiment demonstrated for the first time that coherent ions may be de-activated in an ICR cell by inverting the phase of the excitation voltage. Gäumann et al. applied this finding to excitation pulses over a wide mass range by inserting an incremental delay between two excitation pulses.

The resulting pulse sequence is shown in Fig. 1. $P_1$ and $P_2$ are two identical excitation pulses and $t_1$ the delay between them. During the application of $P_1$, ions are excited and continue to orbit in phase with the voltage of $P_1$ during $t_1$. The phase difference between the ion motion and the radiofrequency voltage of $P_2$ depends on their cyclotron frequency and $t_1$. When ions are in phase with the radiofrequency voltage during $P_2$ ($\Delta\varphi = 2k\pi$), they are excited to a higher radius, but when they are out of phase with $P_2$ ($\Delta\varphi = 2(k+1)\pi$), ions are focused back to the center of the ICR cell, which is consistent with Marshall's experiment.

Gäumann showed that, for a given $m/z$ ratio, the phase difference between the ion motion and the excitation voltage is a linear function of the cyclotron frequency and $t_1$:

$$\Delta\varphi = (\omega_{ion} - \omega_{ref}) \times t_1 + \varphi_0 \quad (1)$$

$\Delta\varphi$ is the phase difference between the ion motion and the excitation voltage, $\omega_{ion}$ is the cyclotron frequency of the ion, $\omega_{ref}$ is a reference frequency (in practice, it corresponds to the highest frequency of the pulse, i.e., the cyclotron frequency of the lowest $m/z$ ratio of the mass range, and is due to the fact that the experiment was performed in heterodyne mode in the second dimension), and $\varphi_0$ is a constant term. As a result, if the experiment is repeated at incremental values of $t_1$, the signal magnitude of the ions is a periodic function of $t_1$ and its frequency is the ions' cyclotron frequency offset by a reference frequency [8].

During the subsequent mixing interval $\tau_m$, fragmentations and ion-molecule reactions are triggered. In Gäumann's first experiments, a reacting gas was introduced in the ICR cell during $\tau_m$ for that goal [2–5], but it was also achieved by pulsing a laser in the ICR cell [5]. The abundance of fragment ions or reaction products depends on the cyclotron radius of the parent ions: in the case of a laser pulse, ions with a high cyclotron radius are outside the laser beam and therefore do not fragment. Only ions that have been de-excited and are therefore in the path of the laser beam can be fragmented. In the case of a reacting gas, the collision frequency

* Corresponding author. Tel.: +33 (0) 320434977; fax: +33 (0) 320336136.
*E-mail address:* christian.rolando@univ-lille1.fr (C. Rolando).

1387-3806/$ – see front matter © 2010 Elsevier B.V. All rights reserved.
doi:10.1016/j.ijms.2010.10.034

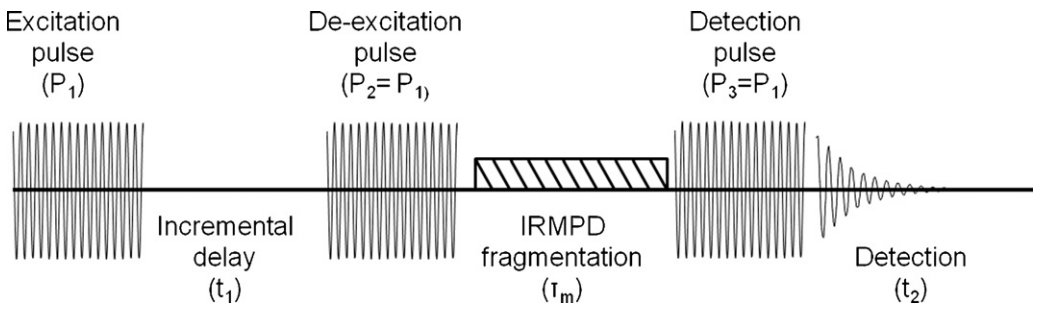


**Fig. 1.** Pulse sequence for a two-dimensional mass spectrometry experiment.

and energy, which determine the reaction yield, depend on the cyclotron radius of the parent ions: the kinetic energy of the ions depends on their cyclotron frequency, and therefore fragmentation rates depend on it, too. In both cases, the abundance of fragment ions depends on the radius of parent ions. The signal magnitude of fragment ions has therefore the same dependency on $t_1$ as the signal magnitude of parent ions.

The subsequent excitation pulse brings parent and fragment ions to a high cyclotron radius and the time transient is detected at the incremented dates $t_2$. The Fourier transform according to $t_2$ gives the spectrum of the cyclotron frequencies of the ions, and the Fourier transform according to $t_1$ gives the modulation frequencies of the abundance of the ions. The resulting two-dimensional spectrum has a characteristic self-correlation line, which reflects the mass spectrum of the sample. The MS/MS parent ion spectrum of each ion species can be read horizontally. The MS/MS fragment ion spectrum of each fragment or product ion can be read vertically. This method was applied by Gäumann et al. for fragmentations by IRMPD and ion-molecule reactions by pulsing a reacting gas during $\tau_m$. They published results for ions of low $m/z$ ratios (<200 amu) using the heterodyne mode in the second dimension and with a narrow mass range ($m/z$ 10–300) and with low resolution in both directions of the spectra: 256 × 1024 data points.

Other methods to record two-dimensional mass spectra have been proposed. Stored-Waveform Ion Radius Modulation (SWIM) was developed by Ross et al. in 1993 in order to modulate ion radii sinusoidally for 2D spectra using CID [9,10]. Hadamard transform FT-ICR/MS, in which a Hadamard comb was applied to an excitation pulse [11–14], was introduced by Williams and McLafferty.

IRMPD is a fragmentation mode that is used extensively in FT-ICR/MS for in-cell MS/MS [15–17]: it is routinely installed on commercial instruments, it does not require gas to be pulsed and therefore does not affect the vacuum in the ICR cell and it is simple to use. While IRMPD does not completely mimic CID, it is efficient, both for odd-electron ions and even-electron ions, and the resulting fragments mostly follow known fragmentation paths.

In this study, we show that the 2D FT-ICR/MS experiment performed by Gäumann et al. with IRMPD is feasible with an external ionization source, with the mass range and mass resolution that have become standard in mass spectrometry in the last 20 years, and with a resolution in the second dimension that had hitherto never been obtained in any 2D FT-ICR/MS experiment. We performed the experiment on a peptide and a peptide mixture and we show that 2D FT-ICR/MS has the potential to become a fully-fledged analytical method that can be used to get extensive structural information on complex samples.

## 2. Experimental methods

Experiments were performed on a 9.4 T ApexQE FT-ICR/MS from Bruker Daltonics (Bremen, Germany) with a positive nanoESI ion source. The peptides used in this study were angiotensin I, substance P and fragments 1–8 of bradykinin purchased from Sigma–Aldrich (Saint Louis, MO, USA) and dissolved in a 50:50 methanol/water mixture with 0.1% formic acid.

The first sample was composed of angiotensin I alone at 1 pmol/μL, and the second sample was a mixture of all thee peptides at 1 pmol/μL each. The methanol and formic acid were obtained from Merck (Darmstadt, Germany) and the water was deionized with a MilliQ water filter system purchased from Millipore (Billerica, MA, USA). The samples were injected in the nanoESI ion source at a 200 nL/min flow rate using a 100 μL syringe (Hamilton, Bonaduz, Switzerland) and an automated syringe pump (Cole Parmer, Vernon Hills, Ill, USA). Ions were accumulated for 1.0 s in the accumulation octopole before being transferred to the ICR cell.

The event sequence and the acquisition of spectra were controlled with the Apex Control software, in LC mode, using a modified pulse program reflecting the event sequence shown in Fig. 1. For the purpose of this study, all pulses were identical in duration, amplitude and frequency range. They were built using the Apex Control (Bruker, Bremen, Germany) pulse generator. Pulse amplitude attenuation was 7.0 dB (i.e., identical to the default pulse amplitude attenuation of excitation pulses) and pulse length was 1.0 μs per frequency (the default excitation pulse length is 20.0 μs per frequency). The frequency list had a 2.0 kHz increment.

Ions were excited and detected over a $m/z$ 86.67–2000 mass range. The length of the time transients was 32,768 data points, which is relatively short for FT-ICR/MS experiments. This choice was imposed by data processing considerations: the programs used in order to calculate the Fourier transforms, being designed for NMR, were not able to handle very large data files due to its 32 bit implementation.

The two-dimensional mass spectra presented in this study were obtained with IRMPD as a fragmentation mode using a continuous $CO_2$ laser with a 10.6 μm wavelength and 25 W power. The laser power and the pulse length were computer-controlled. Experiments were conducted at 50% laser power and $\tau_m$ = 100 ms. The delay between the two first pulses varied with a 0.3 μs increment, giving a Nyquist frequency of 1667 kHz in the second dimension. 2048 transients of 32,768 data points were acquired and stored as a binary file, allowing the same $m/z$ range (86.67–2000) to be detected in both dimensions. The receiver that processed the acquired ion signal had a 3 kHz–10 MHz frequency range.

The data files were imported and Fourier transformed using NPK (NMR Processing Kernel), a program developed for the data analysis of NMR data [18]. The Fourier transform was adjusted to FT-ICR/MS experiments: no phase correction was performed on the data, and the modulus was applied to the result. The spectra were plotted using NMRNotebook 2.60, a software purchased from NMRTec (Illkirch-Graffenstaden, France) and developed to process, visualize and analyze 1D and 2D NMR spectra.

A simulation of the 2D parent ion spectrum of $m/z$ 433 ($f$ = 333 kHz) was undertaken using the Fast Fourier Transform

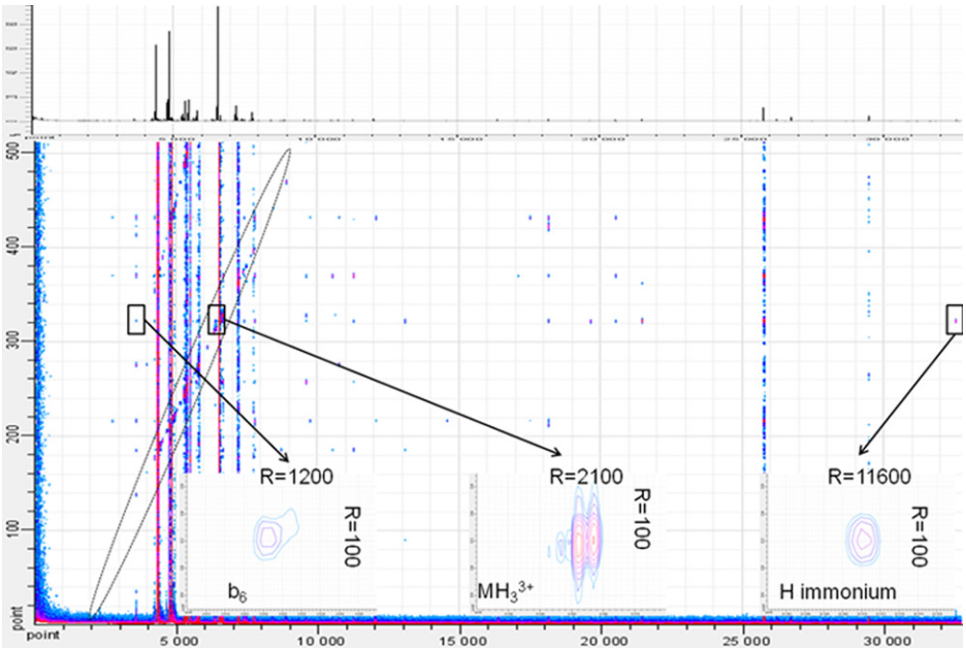


**Fig. 2.** 2D IRMPD mass spectrum of angiotensin I (1 pmol/μL in MeOH/water with 0.1% formic acid) using IRMPD (50% for 0.1 s). Cyclotron frequencies are represented horizontally ($f_{Nyquist}$ = 1667 kHz = 32,768 a.u., corresponding to a $m/z$ 86–2000 mass range) and correlation frequencies are represented vertically ($f_{Nyquist}$ = 1667 kHz = 2048 a.u., corresponding to a $m/z$ 86–2000 mass range). Although the size of the datafile is 32,768 × 2048, we chose to represent 32,768 × 512 for better visibility. Inserts: Self-correlation peak of $MH_3^{3+}$ ($m/z$ 433) with its $^{13}C$ isotopes and resolution of the peak in both directions. Correlation peaks of $MH_3^{3+}$ and $b_6$ ($m/z$ 784) and H immonium ($m/z$ 110) and resolution of the peaks in both dimensions.

macro of Microsoft Office Excel 2007. The calculation was done over 4096 points, but only 2048 of these were retained due to the mirror effect of the Fast Fourier Transform function. The sampling step for this calculation was 0.3 μs, and $m/z$ 433 was assumed to have a 100% fragmentation efficiency at the center of the ICR cell.

The MS/MS spectra of angiotensin I were obtained after ion isolation in the quadrupole and with standard conditions for FT-ICR/MS and with the same fragmentation conditions as the 2D mass spectra: IRMPD at 50% for 100 ms. They were calibrated internally with a single point calibration function in the Data Analysis software provided by Bruker Daltonics (Bremen, Germany).

## 3. Results and discussion

The pulse sequence used in the present study was very similar to the one use by Gäumann et al. [4], except for the fact that there was no carrier frequency for the phase of the second RF excitation pulse and the electronics were completely digital. As a result, the phase difference between the ion motion and the RF excitation voltage is expressed slightly differently from Eq. (1):

$$\Delta\varphi = \omega_{ion} \times t_1 + \varphi_0 \quad (2)$$

The phase difference no longer depended on the reference frequency $\omega_{ref}$, but the theory behind the experiment was still the same.

Although writing the pulse program implementing the pulse sequence presented in Fig. 1 was fairly straightforward, various parameters needed to be optimized in order to obtain a viable 2D mass spectrum. The frequency ranges of the RF excitation pulses determined the mass range in both directions: $P_1$ and $P_2$ had to be identical [19], but the mass range of the excited parent ions (determined by $P_1$ and $P_2$) was not required to be identical to the detected mass range (determined by $P_3$). The frequency range of $P_1 = P_2$ had to be determined according to the mass range of the ions that are injected in the ICR cell (parent ions). $P_3$ needed to be determined according to the mass range of the expected fragment ions. The frequency range of $P_3$ could be wider than the frequency range of $P_1$ and $P_2$. For the purpose of this study, however, we chose identical frequency ranges for all the pulses. The exact pulse program can be found in the supplementary material.

The two-dimensional mass spectrum of angiotensin I shown in Fig. 2 was taken over 2048 × 32,768 data points, which means we measured 2048 time transients of 32,768 data points. In terms of signal modulation, a dataset of 2048 time transients had a resolution that is 4 times higher than the 2D mass spectra obtained with other studies. However, 32,768 data points was very short for a time transient in modern FT-ICR/MS. The necessity of short time transients was brought about by the limited capacity of NMR data processing programs. For the $MH_3^{3+}$ self-correlation peak of angiotensin ($m/z$ 433), we measured that the horizontal resolution was ~2000 and that the vertical resolution was ~100. Both numbers can be improved by increasing the size of the dataset.

In terms of experiment time, a 2048 × 32,768 dataset corresponded to approximately 55 minutes. As a result, 11 pmol of sample were consumed and a data file of 256 Mbytes was generated. While the sensitivity of 2D FT-ICR/MS is not yet comparable to the sensitivity of LC/MS/MS, it will be once we can measure longer time transients. For longer time transients, LC/MS/MS is faster than 2D FT-ICR/MS, but 2D FT-ICR/MS has the potential to be superior in terms of sample coverage, since the 2D mass spectrum contains the fragment ion spectra of all $m/z$ ratios, not only the most abundant ones for a given retention time. Finally, the performance of 2D FT-ICR/MS is not limited by the duty cycle of the mass analyzer like LC/MS/MS is.

The axes of the 2D mass spectrum represent numbers of data points. They can be converted into frequencies with a simple proportionality calculation, since the highest point in the spectrum (32,768 in the horizontal dimension and 2048 in the vertical dimension) corresponds to the Nyquist limit of the experiment (1667 kHz in both dimensions). The horizontal axis represents the Fourier transformed data according to $t_2$ (detection), i.e., the ion cyclotron

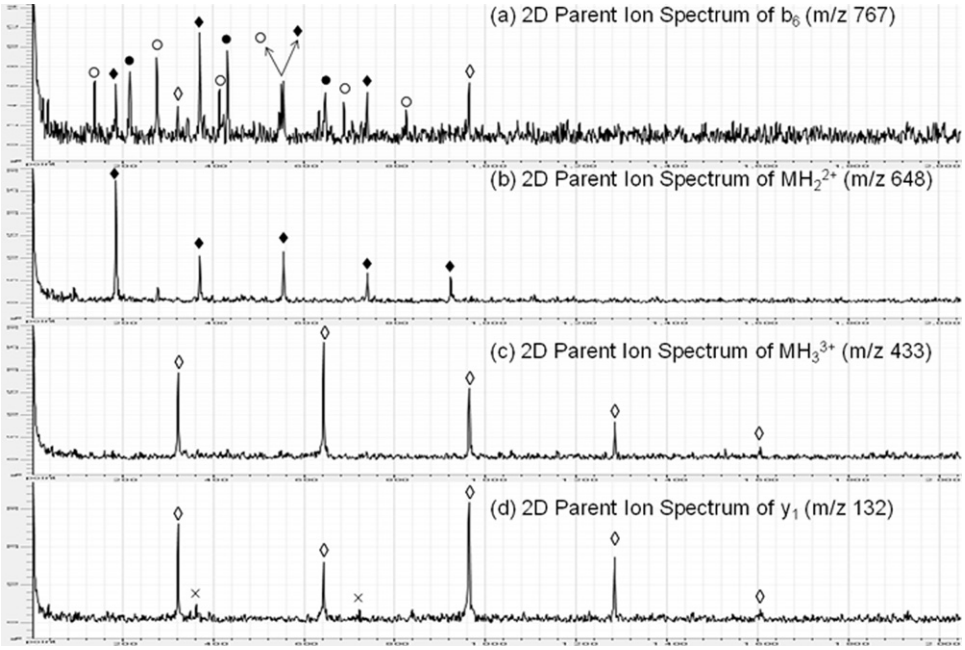


**Fig. 3.** Vertical cuts of the 2D IRMPD mass spectrum of angiotensin shown in Fig. 2. Spectrum (a) shows the parent ions of $m/z$ 767, corresponding to $b_6$ (○: $b_6$, ♦: $MH_2^{2+}$, ●: $b_9^{2+}$, ◊: $MH_3^{3+}$). Spectrum (b) shows the parent ions of $m/z$ 648, corresponding to $MH_2^{2+}$(♦: $MH_2^{2+}$). Spectrum (c) shows the parent ions of $m/z$ 433, corresponding to $MH_3^{3+}$(◊: $MH_3^{3+}$). Spectrum (d) shows the parent ions of $m/z$ 132, corresponding to $y_1$ (◊: $MH_3^{3+}$, ×: $y_9^{3+}$).

frequency spectrum. The $m/z$ ratio can be deduced using the principle of cyclotron motion:

$$\frac{m}{z} = \frac{eB}{2\pi f} \tag{3}$$

in which $e$ is the electric charge of an electron, $B$ the magnetic field and $f$ the frequency. Since the ion radius was different for each time transient and each ion species, we did not calibrate the spectra [20]. The vertical axis represents the Fourier transformed data according to $t_1$ (incremental delay), i.e., the modulation frequency that correlates parent ions and fragment ions.

As a result, we observed several characteristic lines in the 2D mass spectrum. The most important one was a pseudo-diagonal line that showed the self-correlation peaks of the parent ions. For each peak on the self-correlation line (corresponding to the cyclotron frequency of an ion species present in the ICR cell at the start of the experiment) a horizontal line showed the fragment ion spectrum. The vertical line going through any peak showed the parent ion spectrum of the ion species with the corresponding cyclotron frequency.

A major difference between our results and the ideal 2D mass spectrum was the vertical stripes that cross the most abundant peaks on the spectrum. These represented scintillation noise, or $t_1$-noise, as it is known in 2D NMR spectroscopy [21]. Scintillation noise is a non-additive noise that is proportional to the signal and is caused by experimental fluctuations such as the number of ions injected in the ICR cell for each time transient, or phase instabilities of the electronics. Accumulating spectra does not reduce it, and can even increase it. In 2D mass spectra, the level of scintillation noise can be rather high and it can cause errors in spectrum interpretation by creating spurious peaks in fragment ion spectra. In the rest of this study, we will distinguish between the usual thermal noise found in spectra and scintillation noise.

Fig. 3 shows the parent ion spectra of $b_6$, $MH_2^{2+}$, $MH_3^{3+}$ and $y_1$ of angiotensin I. In Fig. 3b and c, we represented the parent ion spectra of $MH_2^{2+}$ and $MH_3^{3+}$: since they were both parent ions that were injected in the ICR cell, the parent ion spectra only showed the self-correlation peaks of these two ions. On both spectra we saw strong harmonics that reflected the various harmonics of the self-correlation line on the 2D mass spectrum. The relative magnitudes of the harmonics were different for $MH_2^{2+}$ and $MH_3^{3+}$ because both signals had different shapes.

In Fig. 3a, we can see the parent ion spectrum of $b_6$. The self-correlation peak was present in the spectrum along with its harmonics, showing that $b_6$ was also present in the MS spectrum of the sample as an in-source fragment. Analysis of the other peaks in the spectrum showed that $b_6$ was a fragment of $MH_2^{2+}$, $MH_3^{3+}$ and $b_9^{2+}$, which is consistent with peptide fragmentation rules. In Fig. 3b, we saw the parent ion spectrum of $y_1$, which did not show a self-correlation peak, but only correlations with $MH_3^{3+}$ and $y_9^{3+}$. We could therefore conclude that $y_1$ was not present among the ions injected in the ICR cell at the beginning of the experiment, but was a product of the in-cell IRMPD fragmentation of $MH_3^{3+}$ and $y_9^{3+}$, which were both present at the start of the experiment.

The presence of harmonics unnecessarily complicated the parent ion spectra: in each parent ion spectrum, the number of peaks was much larger than the number of parent ions, which complicated data interpretation. However, the presence of harmonics provided us with a way to confirm correlation peaks when the signal-to-noise ratio was low. An example of this can be found in the parent ion spectrum of $y_1$: the correlation between $y_1$ and $y_9^{3+}$ had a very low signal-to-noise ratio, but the presence of a harmonic made it possible to confirm its existence.

The vertical harmonics were represented in the 2D mass spectrum as secondary self-correlation lines and secondary fragment ion spectra. They were caused by the fact that, since the signal according to $t_1$ was not shaped like a sinusoid, the Fourier transform contained multiple harmonics of the base frequencies. Guan and Jones [8] showed that the ion cyclotron radius at the end of the second RF excitation pulse can be expressed like:

$$r_A = r_0\sqrt{2(1+\cos\omega_0(T-t_1))} \tag{4}$$

where $r_0$ is the ion cyclotron radius after one RF excitation pulse of length $T$, $\omega_0$ the ion modulation frequency (which is equal to the cyclotron frequency) and $t_1$ the delay between the two first pulses. If the IRMPD laser is thin enough compared to $r_0$, then we can

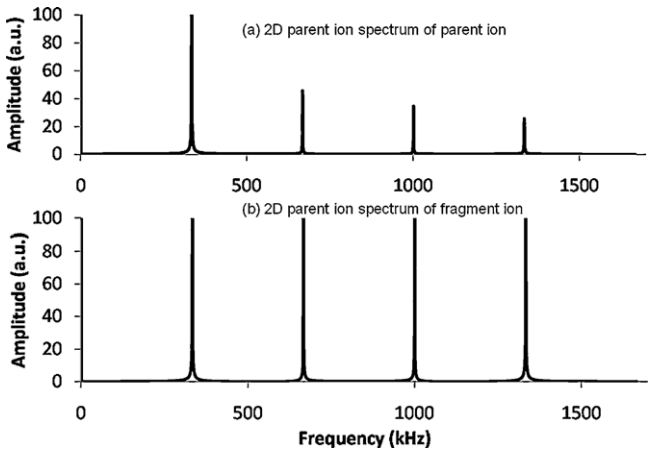


**Fig. 4.** Simulation of (a) the 2D parent ion spectrum of $MH_3^{3+}$ and (b) the 2D parent ion spectrum of a fragment of $MH_3^{3+}$ for 2048 points in the second dimension and a 1667 kHz Nyquist frequency.

posit that the parent ion abundance at the end of the fragmentation period is:

$$\begin{cases} A = A_0 & \text{if } r_A > 0 \\ A = xA_0 & \text{if } r_A = 0 \end{cases} \quad (5)$$

where $A_0$ is the initial parent ion abundance and $0 < x \leq 1$ is the fragmentation efficiency. This is, of course, an approximation, since the influence of the ion packet size and the cross-section of the laser are neglected, but for IRMPD, it is sufficient. At the end of the third RF excitation pulse, the ion cyclotron radius can be expressed as:

$$r_A = r_0 \left(1 + \sqrt{2(1 + \cos \omega_0 (T - t_1))}\right) \quad (6)$$

and the parent ion signal can be expressed as the product of the parent ion abundance and the ion cyclotron radius.

Fig. 4a shows the Fourier transform of this model for the parent ion signal of $MH_3^{3+}$ of angiotensin 1, with a fragmentation efficiency $x = 1$ (this is close to reality, since the MS/MS spectrum of $MH_3^{3+}$ in the same irradiation conditions as the 2D mass spectrum showed no parent ion peak). Harmonics of the self-correlation peak were present, although the relative intensities of the harmonics did not fit with the experimental data. This can be due to the approximations we made: the electric field in the ICR cell during the RF excitation pulses was not uniform and the phase difference between the ion cyclotron motion and the RF excitation voltage was not taken into account when calculating the radius at the end of the third RF excitation pulse.

The presence of harmonics for the ion fragment signal is due to the fact that the abundance of fragment ions depends solely on the cyclotron radius of the parent ion during the fragmentation interval: either the cyclotron radius of the parent ion is larger than the irradiation radius of the laser, and there are no fragment ions, or the parent ion is within the irradiation radius of the laser, and fragmentations occur. In the case where the irradiation radius of the laser is much smaller than the excitation radius $r_0$, the fragment ion signal according to $t_1$ resembles a Dirac comb. As a result, the abundance of a fragment ion can be expressed in the following way:

$$\begin{cases} A = A_0 & \text{if } r_A > 0 \\ A = yA_0 & \text{if } r_A = 0 \end{cases} \quad (7)$$

where $A$ is the abundance of the fragment ion, $y$ its fragmentation efficiency and $r_A$ the cyclotron radius of the parent ion.

The Fourier transform of this signal is a Dirac comb, as shown in Fig. 3b, and it explains the strong presence of harmonics in the second dimension of the 2D mass spectrum. In the 2D mass spectrum, these harmonics translated into secondary horizontal fragmentation lines.

The 2D mass spectrum in Fig. 2 shows the fragmentation patterns of angiotensin I after electrospray ionization. The main parent ions were $MH_2^{2+}$ and $MH_3^{3+}$, but there were also a number of in-source fragments present in the MS spectrum ($b_9^{2+}$, $y_4$, $y_8^{2+}$, $y_9^{3+}$ are the main in-source fragments). We chose not to change the ionization conditions that lead to their formation in order to simulate a complex sample. In this study, we chose to compare $MH_2^{2+}$ and $MH_3^{3+}$: both ions had significantly different abundances in the mass spectrum ($MH_3^{3+}$ was about 10 times more abundant than $MH_2^{2+}$), and for the fragmentation conditions in this study, they had very different behaviors.

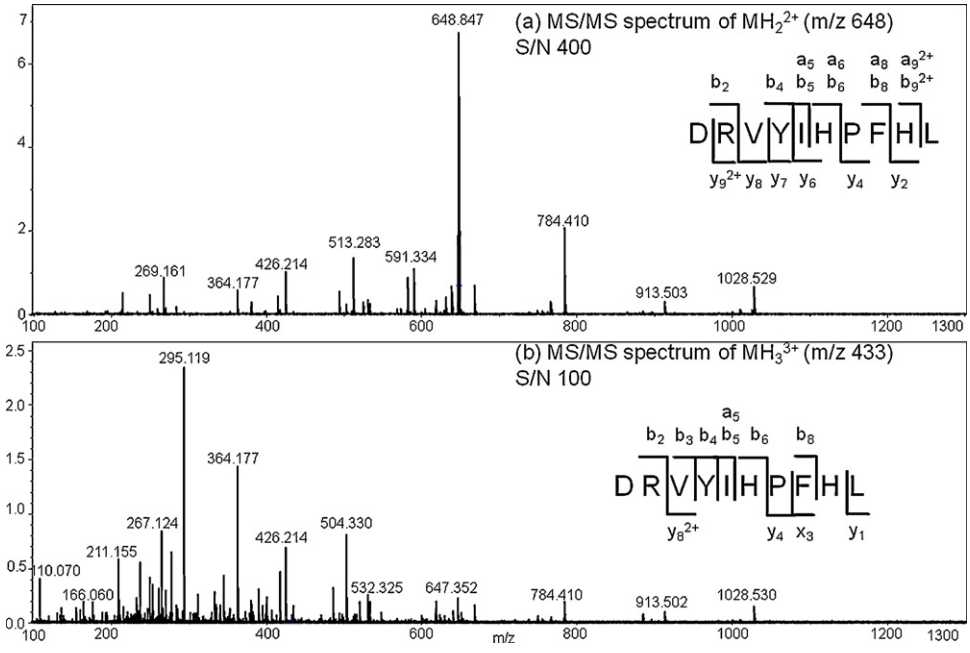


**Fig. 5.** MS/MS spectra of (a) $MH_2^{2+}$ and (b) $MH_3^{3+}$ of angiotensin I with 0.1 s IRMPD at 50% laser power.

**Table 1**
Identification and relative abundance of fragment ions of $MH_3^{3+}$ common to the MS/MS spectrum of Fig. 5b, the 2D fragment ion spectrum of Fig. 6b and the 2D fragment ion spectrum of Fig. 7.

| *m/z* | ppm[a] | Fragment identification | Relative abundance in the MS/MS spectrum (%) | Relative abundance in the 2D mass spectrum of angiotensin (%)[b] | Relative abundance in the 2D mass spectrum of the peptide mixture (%)[b] |
|---|---|---|---|---|---|
| 784.4104 | 0.5 | $b_6$ | 8.2 | 0.4 (6.7) | |
| 669.3835 | 0.5 | RVYIH | 6.7 | 0.5 (8.3) | |
| 626.3047 | | | 1.8 | 0.3 (5.0) | |
| 619.3572 | 1.6 | $a_5$ | 8.4 | 0.3 (5.0) | |
| 532.3250 | 0.9 | RVYI | 11 | 1.2 (20) | |
| 513.2816 | 0.7 | $y_8^{2+}/y_4$ | 2.4 | 2.2 (36.7) | |
| 504.3298 | 0.9 | RVYI-28 | 35 | 0.4 (6.7) | |
| 495.2723 | 1.8 | IHPF | 3.8 | 0.5 (8.3) | |
| 442.2091 | 1.3 | $x_3$ | 1.2 | 0.8 (13.3) | |
| 427.2182 | | | 7.3 | 0.7 (11.7) | |
| 426.2142 | | | 30 | 1.1 (18.3) | 1.1 (23.9) |
| 382.1874 | 0.0 | HPF or PFH | 7.2 | 0.6 (10.0) | 0.4 (8.7) |
| 364.1772 | | | 62 | 0.9 (15.0) | |
| 295.1192 | | | 100 | 0.4 (6.7) | |
| 269.1608 | 0.0 | $y_2$ | 2.6 | 0.2 (3.3) | |
| 263.1390 | 0.0 | VY | 13 | 0.3 (5.0) | |
| 251.1500 | 1.1 | IH | 18 | 0.5 (8.3) | |
| 156.0761 | | | 5.9 | 0.8 (13.3) | |
| 138.0656 | 4.3 | H | 5.8 | 0.5 (8.3) | 0.4 (8.7) |
| 132.1014 | 3.7 | $y_1$ | 3.6 | 2.4 (40) | 2.2 (47.8) |
| 110.0707 | 5.4 | H immonium ion | 17 | 6.0 (100) | 4.6 (100) |
| 87.1476 | | | 4.3 | 1.3 (21.7) | 0.9 (19.6) |

[a] The *m/z* ratios and mass precisions were measured for the MS/MS spectra, after internal calibration.
[b] The first number is taken relative to the highest peak in the horizontal spectrum (i.e., the self-correlation peak of $MH_3^{3+}$) and the number inside the brackets is taken relative to the highest fragment peak in the spectrum.

As we can see in Fig. 5, which shows the MS/MS spectra of $MH_2^{2+}$ and $MH_3^{3+}$ at 50% laser fluence for 0.1 s, $MH_2^{2+}$ did not fragment very efficiently, and the parent ion was also the most abundant ion in the spectrum (see Fig. 5a). We observed $b_9^{2+}$ and $y_9^{2+}$ fragments but no $b_9$ or $y_9$ fragments, in accordance with what has been reported previously in literature [22,23]. We also observed $a_5$, $a_6$, $a_8$ and $a_9^{2+}$ fragments. $MH_3^{3+}$ underwent a coulombic explosion, yielding high abundance $x_3$ ions, as well as $a_5$ ions, in addition to b and y ions (see Fig. 5b).

Table 1 lists the fragments of $MH_3^{3+}$ that were both in the 2D mass spectrum and in the MS/MS spectrum. The fragments were identified using ProteinProspector. Most fragments found in the 2D mass spectrum could be found in the MS/MS spectrum except for three of them, whose *m/z* ratio were close to the *m/z* ratios of $b_7^{2+}$, $(b7–H_2O–NH_3)^{2+}$ and $y_9^{3+}$. We also found that there is no close correlation between the relative abundance of the ions in the 2D fragment ion spectrum and the MS/MS spectrum.

Fig. 6 shows the fragment ion spectra of $MH_2^{2+}$ and $MH_3^{3+}$ in the 2D mass spectrum. Both spectra had very high signal-to-noise ratios (over 500 for $MH_3^{3+}$ and $MH_2^{2+}$). They showed a significant number of fragments that ensured almost complete coverage of the peptide, together with numerous internal fragments. However, the relative abundance of the fragments did not exceed 10% of the self-correlation peaks and was lower than the level of scintillation noise of the main parent ions. This may be caused by the fact that parent ions were excited to a higher radius than fragment ions: when they were at their maximum radius, parent ions were submitted to the equivalent of a 3.0 μs RF excitation pulse, whereas fragment ions were submitted to an RF excitation pulse of only 1.0 μs. The difference in relative abundances between parent and fragment ion peaks is therefore not surprising.

The performances of the 2D fragment ion spectra of $MH_2^{2+}$ and $MH_3^{3+}$ (Fig. 6) and their MS/MS spectra (Fig. 5) are listed in Table 2. In order to rate the quality of the spectra, we wish to distinguish the concepts of signal-to-noise ratio and sensitivity: signal-to-noise ratio is the ratio between the amplitudes of the highest peak and the average level of noise, and sensitivity is the number of verified peaks that come out of the noise, compared to the number of peaks that are present in the relevant MS/MS spectra. The signal-to-noise ratio was significantly higher for the fragment ion spectra than the MS/MS spectra because many more time transients were measured for each data point in the 2D mass spectrum than in the MS/MS spectrum. Sensitivity, however, was much higher for the MS/MS spectra than for the 2D fragment ion spectra.

The number of peaks that were detected in the MS/MS spectra was much higher than the number of peaks detected in the 2D fragment ion spectra. One obvious explanation for this is the length of the RF excitation pulse and of the time transients. The MS/MS spectra were measured in the default conditions of the instrument: 20 μs RF excitation pulses and 512k time transients. The 2D mass spectrum, however, was measured with an RF excitation pulse of a maximum 3 μs length (1 μs for each RF pulse). As a result, the ion signal was much lower because the maximum cyclotron radius of the ions was much smaller. Unfortunately, we did not observe any fragment ion peaks in 2D mass spectra using RF pulses that were longer than 1 μs. The memory limitations of the data processing software restricted the length of the time transients to 32k, which also contributed to the low number of peaks observed in the 2D mass spectrum.

Fig. 7 shows the 2D mass spectrum of an equimolar mixture of angiotensin I, bradykinin and substance P. In the MS spectrum of this sample, the peaks of $MH_2^{2+}$ and $MH_3^{3+}$ of angiotensin were respectively at 3 and 22% of relative abundance. Because of the

**Table 2**
Characteristics of the MS/MS spectra and of the fragment ion spectra in the 2D mass spectrum of angiotensin I alone and of a peptide mixture for $MH_2^{2+}$ and $MH_3^{3+}$ as parent ions.

| | $MH_2^{2+}$ | $MH_3^{3+}$ |
|---|---|---|
| S/N ratio | | |
| MS/MS | 400 | 100 |
| 2D | 500 | 500 |
| 2D of mixture | 80 | 300 |
| Number of peaks | | |
| MS/MS | 194 | 367 |
| 2D (in common with MS/MS) | 12 (12) | 25 (22) |
| 2D of mixture (in common with 2D of angiotensin alone) | 0 (0) | 10 (10) |

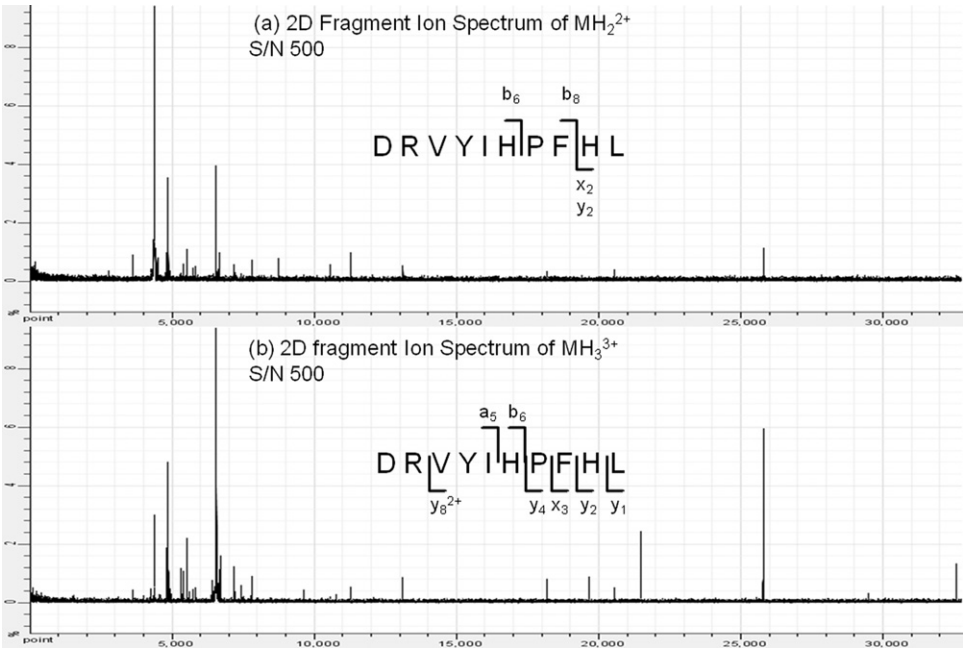


**Fig. 6.** Horizontal cuts of the 2D IRMPD mass spectrum of angiotensin I represented in Fig. 2. Spectrum (a) shows the fragment ions $MH_2^{2+}$ ($m/z$ 648) and spectrum (b) shows the fragment ions of $MH_3^{3+}$ ($m/z$ 433). For $MH_2^{2+}$ we identified the following fragments: $b_8$, $b_6$, $(MH\text{-}H_2O)^{2+}$, IHPFH. For $MH_3^{3+}$ we identified the following fragments: $b_6$, RVYIH, $a_5$, $y_4$, $y_8^{2+}$, RVYI-28, IHPF, $x_3$, HPF/PFH, $y_2$, IH, H, $y_1$ and H (immonium ion).

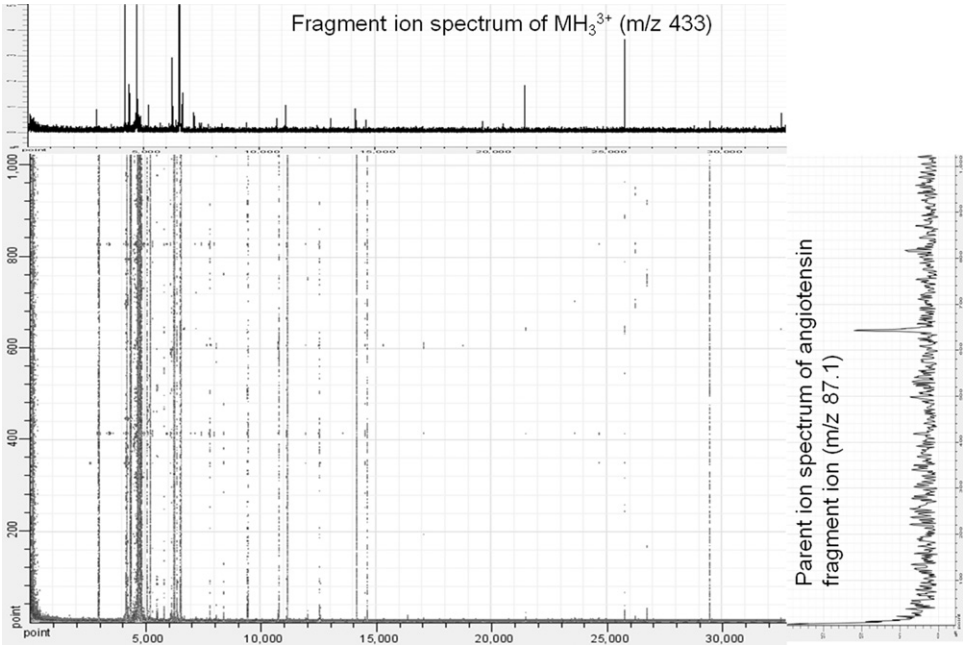


**Fig. 7.** 2D IRMPD mass spectrum of a mixture of angiotensin I, substance P and bradykinin (1 pmol/μL each in MeOH/water with 0.1% formic acid) using IRMPD (50% for 0.1 s). Cyclotron frequencies are represented horizontally ($f_{Nyquist}$ = 1667 kHz = 32,768 a.u., corresponding to a $m/z$ 86–2000 mass range) and correlation frequencies are represented vertically ($f_{Nyquist}$ = 1667 kHz = 2048 a.u., corresponding to a $m/z$ 86–2000 mass range). Although the size of the datafile is 32,768 × 2048, we chose to represent 32,768 × 1024 for better visibility. Inserts: 2D fragment ion spectrum of $MH_3^{3+}$ of angiotensin (top), 2D parent ion spectrum of fragment ion $m/z$ 87.1 of angiotensin (right).

lower ion abundance in the MS spectrum, the signal-to-noise ratios of the fragment ion spectra of $MH_2^{2+}$ and $MH_3^{3+}$ were lower than in the 2D spectrum of angiotensin alone (Table 2). We also noticed that the number of fragment ions of both $MH_2^{2+}$ and $MH_3^{3+}$ decreased. However, the relative abundance of the fragment ion peaks of the mixture was comparable to the relative abundance of the fragment ion peaks of angiotensin alone (Table 1). Fragment ion peaks were properly visible on the 2D mass spectrum and the signal-to-noise ratio of the parent ion spectra was high.

## 4. Conclusion

In this study, we implemented Gäumann's 2D mass spectrometry experiment on a commercial FT-ICR instrument, with successful results. We were able to measure the 2D spectrum of a peptide and of a mixture of peptides over an analytically useful mass range, with a gas-free fragmentation mode that allowed us to measure 2D mass spectra without the loss in sensitivity and resolution that occurs when a gas is pulsed in the ICR cell.

A number of problems still need to be addressed, however, before 2D mass spectrometry becomes a viable analytical method. First, the size of the datasets needs to be increased in order to maintain the sensitivity and the resolving power of FT-ICR technology. This problem is easily solved by improving existing NMR data processing programs and adapting them to FT-ICR/MS. Other problems are less simple to solve: the acquisition time and the amount of sample needed for one 2D mass spectrum are both very high, and it is important to minimize them in the development of a sensitive analytical tool. The scintillation noise is also an important problem that needs to be addressed in order to prevent errors in the interpretation of the 2D mass spectra. The relative magnitude of the self-correlation peaks and the off-diagonal fragment peaks is important as well in terms of sensitivity.

The encouraging factor is that all of these problems have already been solved for 2D NMR spectroscopy and only need to be adapted to 2D mass spectrometry. Acquisition time and sample quantities can be reduced by using partial sampling techniques combined with Maximum Entropy methods [24]. There are also several methods to reduce or eliminate scintillation noise, like the aforementioned Maximum Entropy methods, or using the Cadzow algorithm [25,26] in order to reduce the noise on the vertical dimension. We can also use covariance analysis [27,28] in order to reduce noise and to eliminate the self-correlation peaks, which would enhance the visibility of off-diagonal fragment peaks. While 2D FT-ICR/MS has yet to become a viable method of chemical analysis, it holds great promise that can be realized by exploring the various methods that have been built for 2D NMR spectroscopy. Technological advances in computer science make it possible to apply the methods that were developed for the relatively small datasets in 2D NMR spectroscopy to 2D mass spectrometry in order to obtain sensitive, well-resolved 2D mass spectra that can give us good structural information on complex samples.

## Acknowledgements

The FT-ICR mass spectrometer and the Proteomics Platform used for this study are funded by the European community (FEDER), the Région Nord-Pas de Calais (France), the IBISA network, the CNRS and the Université de Lille 1, Sciences et Technologies which are gratefully acknowledged. M.v.A. thanks the Région Nord Pas-de-Calais for post-doc funding.

## Appendix A. Supplementary data

Supplementary data associated with this article can be found, in the online version, at doi:10.1016/j.ijms.2010.10.034.

## References

[1] A.G. Marshall, C.L. Hendrickson, Int. J. Mass Spectrom. 215 (2002) 59.
[2] P. Pfaendler, G. Bodenhausen, J. Rapin, R. Houriet, T. Gaeumann, Chem. Phys. Lett. 138 (1987) 195.
[3] P. Pfaendler, G. Bodenhausen, J. Rapin, M.E. Walser, T. Gaeumann, J. Am. Chem. Soc. 110 (1988) 5625.
[4] G. Bodenhausen, P.E. Pfaendler, J. Rapin, T. Gaumann, R. Houriet, US Patent 88-198975 (1989).
[5] M. Bensimon, G. Zhao, T. Gäumann, Chem. Phys. Lett. 157 (1989) 97.
[6] A.G. Marshall, T.C.L. Wang, T.L. Ricca, Chem. Phys. Lett. 105 (1984) 233.
[7] A. Kumar, R.R. Ernst, K. Wuethrich, Biochem. Biophys. Res. Commun. 95 (1980) 1.
[8] S. Guan, P.R. Jones, J. Chem. Phys. 91 (1989) 5291.
[9] C.W. Ross III, S. Guan, P.B. Grosshans, T.L. Ricca, A.G. Marshall, J. Am. Chem. Soc. 115 (1993) 7854.
[10] C.W. Ross, W.J. Simonsick Jr., D. Aaserud, J. Anal. Chem. 74 (2002) 4625.
[11] F.W. McLafferty, D.B. Stauffer, S.Y. Loh, E.R. Williams, Anal. Chem. 59 (1987) 2212.
[12] E.R. Williams, F.W. McLafferty, US Patent 90-500483 (1990).
[13] X. Gao, T.D. Wood, Rapid Commun. Mass Spectrom. 10 (1996) 1997.
[14] S. Haebel, T. Gaeumann, Int. J. Mass Spectrom. Ion Processes 144 (1995) 139.
[15] N. Garnier, C. Rolando, J.M. Hotje, C. Tokarski, Int. J. Mass Spectrom. 284 (2009) 47.
[16] M. Schaefer, M.K. Drayss, D. Blunk, J.M. Purcell, C.L. Hendrickson, A.G. Marshall, A. Mookherjee, P.B. Armentrout, J. Phys. Chem. A 113 (2009) 7779.
[17] M. Ma, R. Chen, Y. Ge, H. He, A.G. Marshall, L. Li, Anal. Chem. (Washington, DC, U.S.) 81 (2009) 240.
[18] D. Tramesel, V. Catherinot, M.-A. Delsuc, J. Magn. Reson. 188 (2007) 56.
[19] M.V. Gorshkov, E.N. Nikolaev, Int. J. Mass Spectrom. Ion Processes 125 (1993) 1.
[20] S.D.H. Shi, J.J. Drader, M.A. Freitas, C.L. Hendrickson, A.G. Marshall, Int. J. Mass Spectrom. 195/196 (2000) 591.
[21] A.F. Mehlkopf, D. Korbee, T.A. Tiggelman, R. Freeman, J. Magn. Reson. 58 (1984) 315.
[22] M.C. Crowe, J.S. Brodbelt, J. Am. Soc. Mass Spectrom. 15 (2004) 1581.
[23] K. Fukui, Y. Naito, Y. Akiyama, K. Takahashi, Int. J. Mass Spectrom. 235 (2004) 25.
[24] M.-A. Delsuc, D. Tramesel, C. R. Chim. 9 (2006) 364.
[25] J.A. Cadzow, M.M. Wu, IEE Proceedings Pt. F 134 (1987) 69.
[26] C. Brissac, T.E. Malliavin, M.A. Delsuc, J. Biomol. NMR 6 (1995) 361.
[27] R. Bruschweiler, J. Chem. Phys. 121 (2004) 409.
[28] M. Weingarth, P. Tekely, R. Brueschweiler, G. Bodenhausen, Chem. Commun. (Cambridge, U.K.) 46 (2010) 952.